Research Article BEU Fen Bilimleri Dergisi 15(1): 373-393 (2026) DOI: 10.17798/bitlisfen.1817058

BİTLİS EREN UNIVERSITY
FEN BİLİMLERİ DERGİSİ
ISSN: 2147-3129 / e-ISSN: 2147-3188

EXPERIMENTAL AND NUMERICAL INVESTIGATION OF THE EFFECT OF INSUFFICIENT EDGE DISTANCE ON THE BEHAVIOR OF COLD-FORMED STEEL SCREW CONNECTIONS

Ramazan ORUÇ [1*], Yakup BÖLÜKBAŞ [1]

[1] *Aksaray University, Civil Engineering Department, Aksaray, Türkiye*
**** Corresponding Author:*** ramazanoruc@aksaray.edu.tr

Article Info

Received: *November 4, 2025*
Revised: *February 16, 2026*
Accepted: *February 24, 2026*

Keywords
Cold-formed steel,
Screwed connection,
Edge distance,
Experimental study,
Numerical study.

ABSTRACT

This study investigates the shear behavior of cold-formed steel single-lap screw connections both experimentally and numerically, with a particular focus on the critical influence of edge distance. A total of 20 specimens were tested to evaluate the effects of sheet thickness, screw diameter, number of screws, screw arrangement, and edge distance on connection load-carrying capacity and failure modes. The experimental results showed that increasing the sheet thickness nearly doubled the connection capacity, while the effect of screw diameter was found to be limited. Conversely, a reduction in horizontal edge distance had a critically adverse effect on the connection performance. In addition, detailed finite element models were developed in ABAQUS and validated against the experimental data. The numerical models accurately predicted the load-displacement behavior, load-carrying capacities, and failure modes, demonstrating that they serve as a reliable tool for future parametric studies.

1. INTRODUCTION

Cold-formed steel (CFS) members are becoming increasingly important in modern construction technologies due to their advantages, such as light weight, high strength, ease of assembly, and cost efficiency. These members are produced by plastically deforming thin steel sheets at room temperature. They are considered highly efficient in terms of material utilization, making a significant contribution to the concept of sustainable construction. Today, CFS members are widely used in the structural systems of residential and industrial buildings, as well as in roof and wall assemblies, light steel prefabricated structures, storage buildings, and various infrastructure applications. Thanks to their high strength-to-weight ratio, they provide safe and durable structural solutions, particularly in seismic regions, while also offering an economical alternative through rapid manufacturing and ease of installation.

In the assembly of cold-formed steel (CFS) members, screw connections are commonly preferred. Screws are widely used fastening elements due to their ease of application to thin steel sheets and the practicality of drilling and installation processes. Such connections are frequently employed to attach cold-formed steel channels to structural framing members, as well as to connect continuous channels and steel sheets in roof and wall systems. However, in screw connections subjected simultaneously to shear and bending forces, it has been observed that while some screws reach their ultimate limit state, others remain within the elastic range. Therefore, to accurately evaluate the behavior of complex screw connections, it is essential to investigate the pre-failure load-displacement relationship of these joints in detail [1].

The design of screw connection capacities in cold-formed steel structures has been comprehensively addressed in both European and American standards [2–3]. In both standards, the load-carrying capacity of screw connections is determined using empirical formulations. According to the European standard Eurocode EN 1993-1-3 [2], screw connection design is based on bearing, net-section, and shear behaviors. In contrast, the American standard AISI S100-16 [3] considers tilting, bearing, and shear behaviors in connection design. Since both standards rely on empirical approaches, and because screw

connection behavior depends on numerous parameters and exhibits inherent nonlinearity, further comprehensive research on these joints is necessary. In recent years, the number of studies in this field has increased significantly, and the behavior of cold-formed steel screw connections has become a topic of growing importance among researchers.

Rogers and Hancock [4] proposed a new design equation to more accurately predict the strength of screw connections failing under combined bearing and tilting modes. Similarly, several studies have developed new formulations for determining the load capacity of joints using self-drilling or innovative screw types [5–9]. Research investigating the group effect in multi-screw connections has also indicated that existing standards may not provide sufficient accuracy in strength prediction, and new empirical equations have been proposed to improve reliability [10–12]. Furthermore, numerous experimental studies have examined the behavior of screw connections under elevated temperatures, contributing to a better understanding of their performance under different environmental and loading conditions [13–17].

The main objective of this study is to investigate the shear behavior of cold-formed steel sheets connected with self-drilling screws having insufficient edge distance, through both experimental and numerical approaches. Within the scope of the study, the load-displacement relationships, load-carrying capacities, and failure modes of the specimens were determined under various geometric parameters, screw arrangements, and connection configurations to reveal the influence of self-drilling screws on the connection behavior. The experimental data were compared with numerical models developed using the finite element method (FEA), allowing for the evaluation of the accuracy and reliability of the numerical analyses.

2. MATERIAL AND METHOD

2.1. Testing Specimens

To examine the behavior of single-lap connections in CFS members with screw fasteners, a total of 20 single-lap connection specimens were prepared based on the testing procedure specified in AISI S905 [18]. The cross-sections used in the experiments, which were designed with three different connection layouts, are presented in Figure 1. The geometric and configuration parameters of all test specimens, including screw diameter, sheet thickness, number of screws, and edge distances, are summarized in Table 1.

The specimens were labeled to indicate the number of screws, screw arrangement, screw diameter, vertical edge distance, horizontal edge distance, and sheet thickness. For example, the specimen labeled “1SC55EV30EH15T1/1” represents a single-screw connection with a screw diameter of 5.5 mm, a vertical edge distance (e_1) of 30 mm, a horizontal edge distance (e_3) of 15 mm, and sheet thicknesses of t_1=1 mm and t_2=1 mm. Similarly, the specimen labeled “2SCL55BW60EV30EH15T1/1” represents a two-screw vertical arrangement with a screw diameter of 5.5 mm, a vertical spacing (p_1) of 60 mm, e_1=30 mm, e_3=15 mm, and t_1=t_2=1 mm.

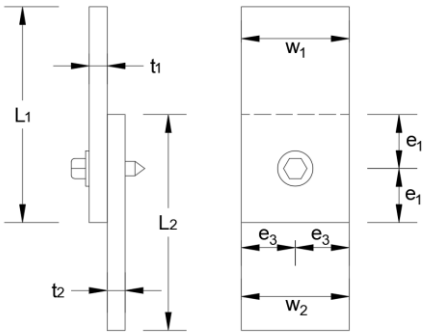

(a)

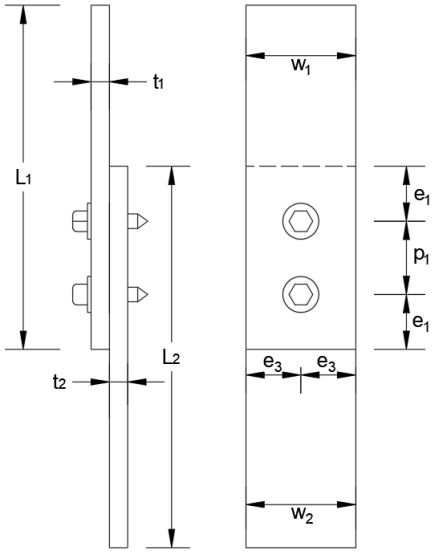

(b)

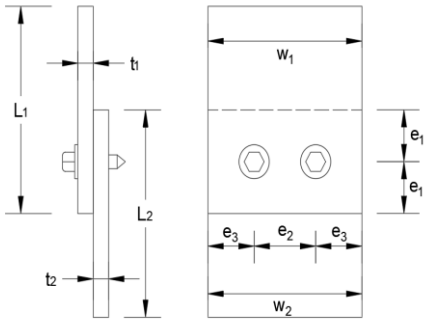

(c)

L_1: Length of the upper plate

L_2: Length of the lower plate

t_1: Thickness of upper plate

t_2: Thickness of lower plate

w_1: Width of upper plate

w_2: Width of lower plate

e_1 : Distance from the screw in the vertical direction to the corner

e_2: Distance between screws in the horizontal direction

e_3: Distance from the screw in the horizontal direction to the corner

p_1: Distance between screws in the vertical direction

Figure 1. The geometric layout of the test specimens.

Table 1. Geometric properties of the test specimens

Specimen	Screw Diameter, d (mm)	Steel thickness t_1-t_2 (mm)	Screw number	w_1=w_2	e_1	e_2	e_3	p_1
1SC55EV30EH15T1/1	5.5	1-1	1	30	30	-	15	-
1SC63EV30EH15T1/1	6.3	1-1	1	30	30	-	15	-
1SC55EV30EH15T2/2	5.5	2-2	1	30	30	-	15	-
1SC63EV30EH15T2/2	6.3	2-2	1	30	30	-	15	-
1SC55EV30EH75T1/1	5.5	1-1	1	15	30	-	7.5	-
1SC63EV30EH75T1/1	6.3	1-1	1	15	30	-	7.5	-
1SC55EV30EH75T2/2	5.5	2-2	1	15	30	-	7.5	-
1SC63EV30EH75T2/2	6.3	2-2	1	15	30	-	7.5	-
2SCL55BW60EV30EH15T1/1	5.5	1-1	2	30	30	-	15	60
2SCL63BW60EV30EH15T1/1	6.3	1-1	2	30	30	-	15	60
2SCL55BW60EV30EH15T2/2	5.5	2-2	2	30	30	-	15	60
2SCL63BW60EV30EH15T2/2	6.3	2-2	2	30	30	-	15	60
2SCL55BW60EV30EH75T1/1	5.5	1-1	2	15	30	-	7.5	60
2SCL63BW60EV30EH75T1/1	6.3	1-1	2	15	30	-	7.5	60
2SCL55BW60EV30EH75T2/2	5.5	2-2	2	15	30	-	7.5	60
2SCL63BW60EV30EH75T2/2	6.3	2-2	2	15	30	-	7.5	60
2SCT55BW10EV30EH20T1/1	5.5	1-1	2	50	30	10	20	
2SCT63BW10EV30EH20T1/1	6.3	1-1	2	50	30	10	20	
2SCT55BW10EV30EH20T2/2	5.5	2-2	2	50	30	10	20	
2SCT63BW10EV30EH20T2/2	6.3	2-2	2	50	30	10	20	

2.2. Material Properties

The test specimens were fabricated from hot-dip galvanized steel sheets of grade DX51D. To determine the mechanical properties of the material, tensile tests were conducted on specimens with thicknesses of 1 mm and 2 mm in accordance with EN ISO 6892-1 [19]. The geometry of the tensile specimens is illustrated in Figure 2.

All tensile tests were carried out using a 600 kN capacity universal testing machine operating under a loading rate of 0.01 mm/s. An extensometer with a 100 mm gauge length was employed to record the elongation of the specimens during testing. The stress–strain relationships obtained from the tests for the 1 mm and 2 mm thick sheets are shown in Figure 2, while their corresponding mechanical properties are summarized in Table 2.

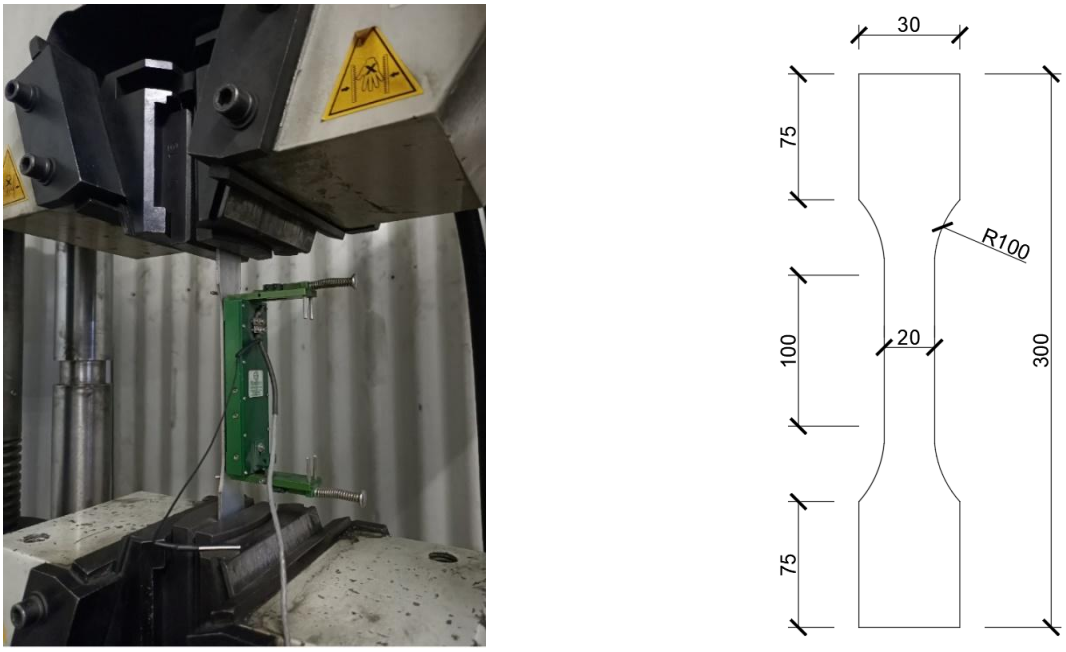

(a) (b)

Figure 2. Tensile testing (a) instrument (b) geometric layout of the tensile test specimen.

Table 2. Material properties for 1 and 2 mm specimens

Tensile Specimens	E_0 (MPa)	σ_{y0} MPa	σ_u	ε_u
1 mm	205400	325.5	360.5	0.17
2 mm	206800	330.5	395.5	0.19

2.3. Testing Procedure

The experiments were carried out using a hydraulic testing setup with a 2000 kN capacity. The applied loads were recorded through a 200 kN capacity load cell integrated into the data acquisition system. During the tests, two Linear Variable Differential Transformers (LVDT) were used to measure and record the displacement of the connections. Additionally, strain gauges were attached near the screw head contact zones on the steel sheet surfaces to measure local strain variations during loading.

The overall configuration of the testing setup is illustrated in Figure 3. Based on the recorded load and displacement data, load-displacement curves were generated for each specimen, and the corresponding results are presented in the Experimental Results section.

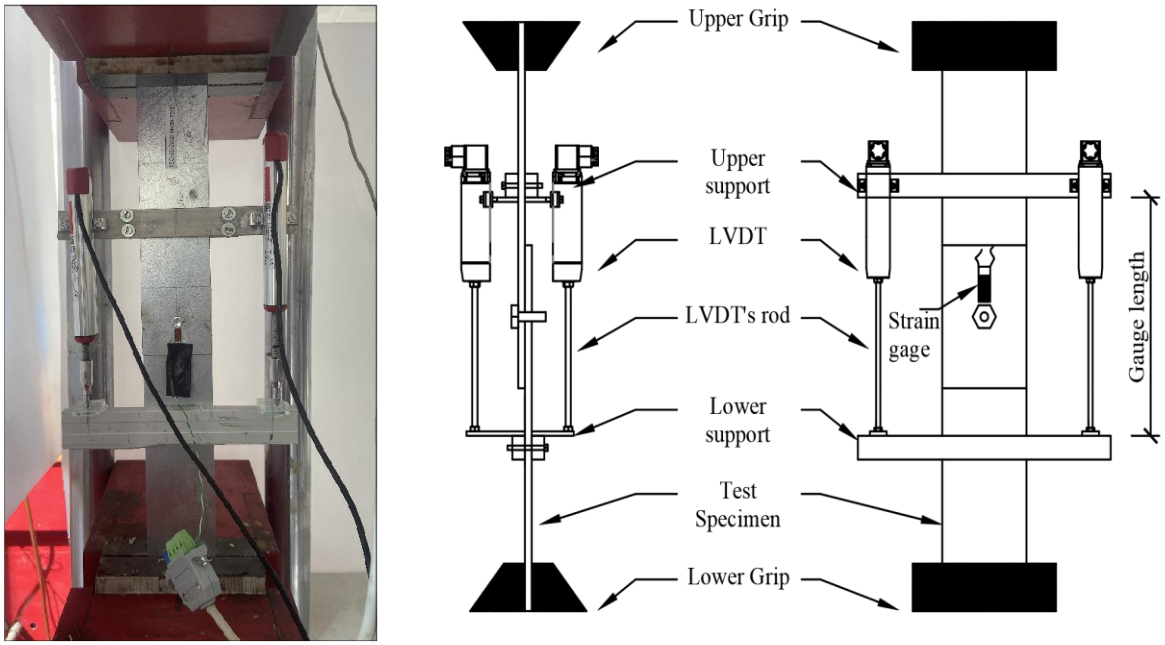

(a) test setup in laboratory (b) details of test setup

Figure 3. Test setup.

3. TEST RESULTS

Within the scope of this study, a total of 20 single-lap connections with self-drilling screws were tested to investigate the effects of screw diameter and edge distance on the load-carrying capacity and failure modes of CFS members. The resulting load-displacement curves from the experiments are presented in Figure 4 (a–e), while the observed failure modes are summarized in Table 3. In Table 3, the failure modes are denoted as follows: “S” for screw shear failure, “T” for screw tilting, “B” for bearing, “P” for screw pull-through, and “NS” for net-section failure.

3.1. Comparison of Load-Carrying Capacity

It was observed that increasing the sheet thickness significantly enhanced the load-carrying capacity of the connections. For instance, in single-screw connections with the same screw diameter and edge distance, increasing the sheet thickness from 1 mm to 2 mm approximately doubled the average connection capacity (e.g., for specimen 1SC55EV30EH15, the capacity increased from 3.95 kN to 7.85 kN). The effect of increasing the screw diameter (from 5.5 mm to 6.3 mm) on the load-carrying capacity was found to be limited. For example, the capacity of specimen 1SC55EV30EH15T1-1 was 3.92 kN, whereas for 1SC63EV30EH15T1-1, it increased slightly to 4.16 kN, representing an approximate 6% increase. The horizontal edge distance (e_3) was found to have a critical influence on the connection capacity. Reducing e_3 from 15 mm to 7.5 mm led to a significant decrease in capacity. In single-screw specimens, the average reduction in capacity was about 38%, while in two-screw specimens it reached approximately 94%. As expected, increasing the number of screws generally enhanced the load-carrying capacity, although this increase was not strictly proportional, likely due to uneven load distribution among the screws. In addition to the uneven load distribution among screws, the non-proportional increase in load capacity with increasing screw number can also be attributed to changes in governing failure modes. Particularly at reduced edge distances, net-section failure may become dominant and limit the overall connection capacity regardless of the number of screws. Moreover, the alignment of screws, whether in vertical alignment (SCL) or horizontal alignment (SCT), also affected the load-carrying performance of the connections.

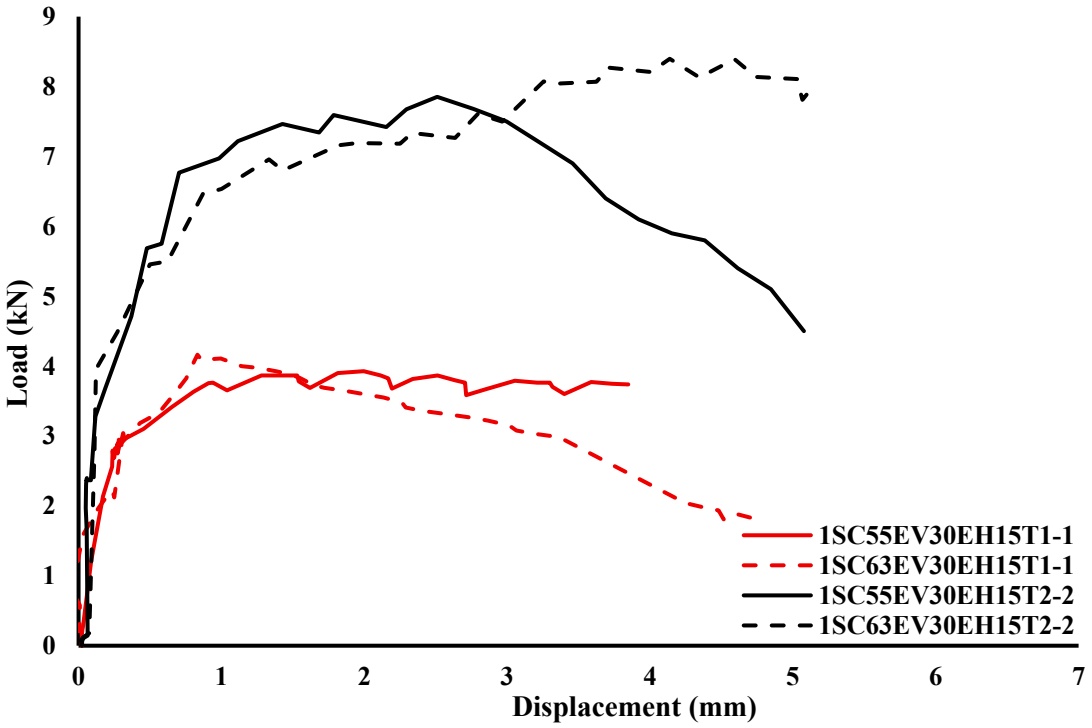

(a) *Test members with a horizontal edge distance of 15 mm*

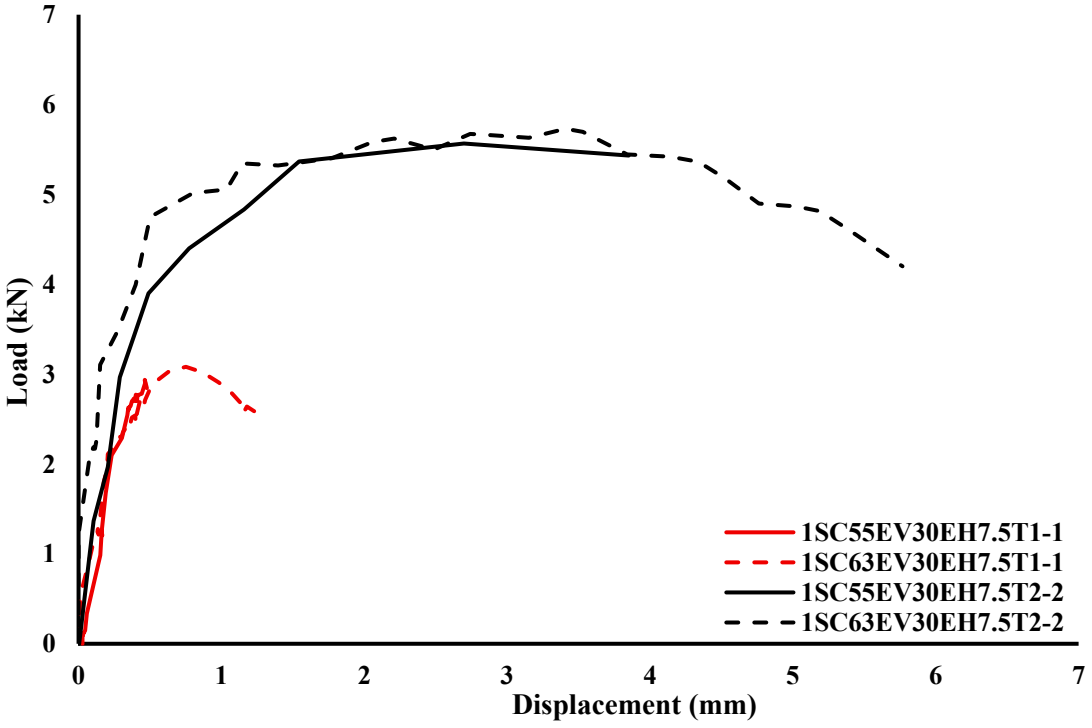

(b) Test members with a horizontal edge distance of 7.5 mm

Figure 4. Comparison of the load–displacement curves of the test members.

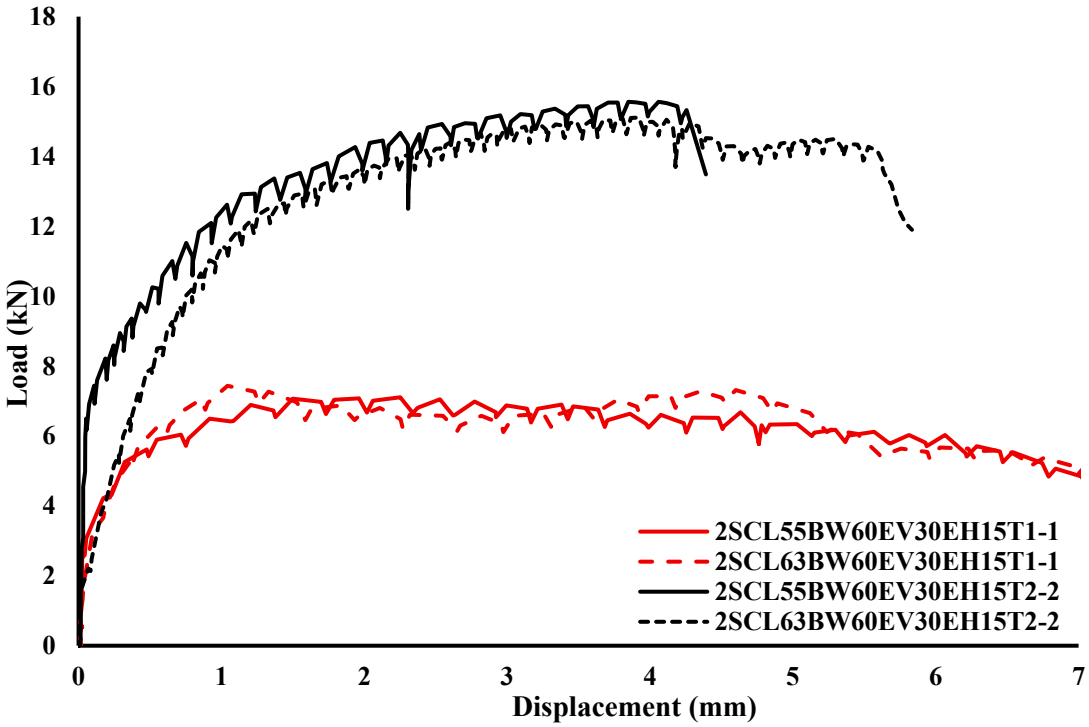

(c) Horizontal edge distance of 15 mm and vertically aligned screw connections

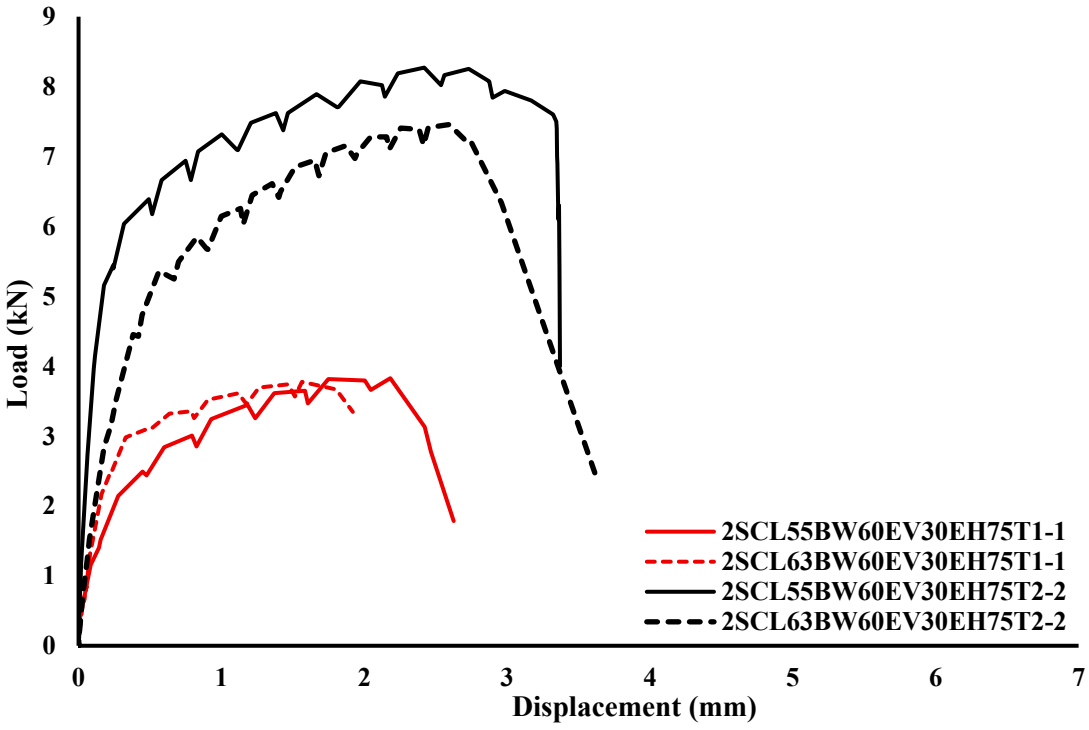

(d) Horizontal edge distance of 7.5 mm and vertically aligned screw connections

Figure 4 (continued). Comparison of the load–displacement curves of the test members

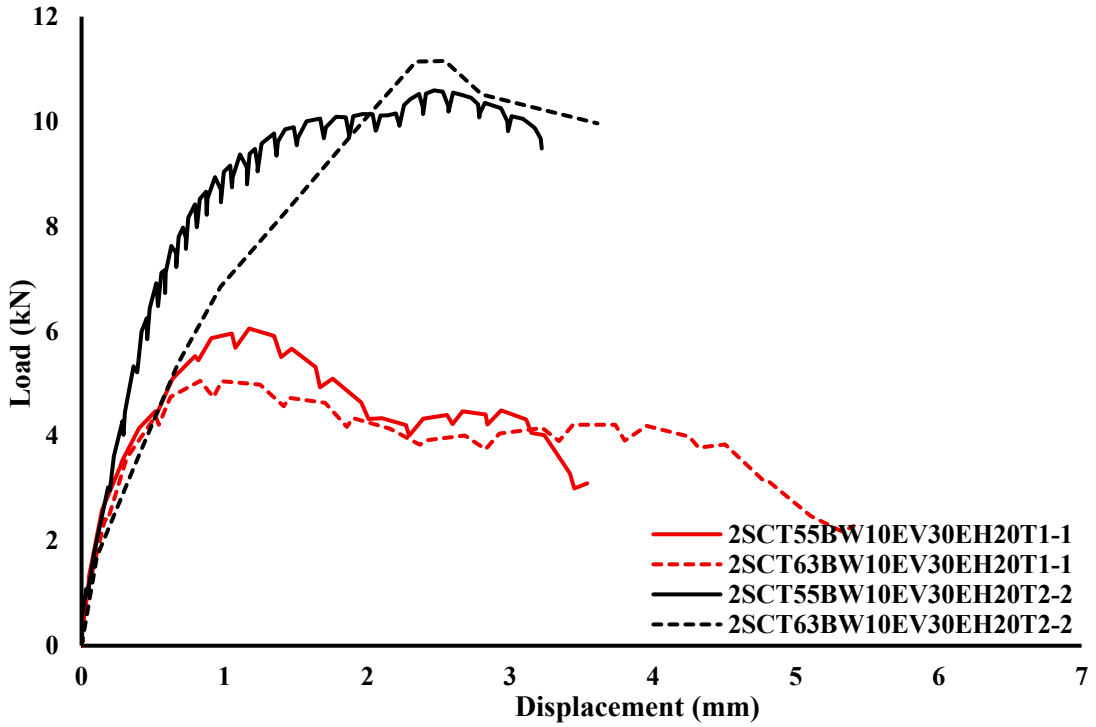

(e) Test members with horizontally aligned screw connections

Figure 4 (continued). Comparison of the load–displacement curves of the test members.

3.2. Comparison of Failure Modes

The observed failure modes from the experiments included screw tilting and bearing (T-B), screw shear (S), screw tilting and shear (T-S), screw tilting and pull-through (T-P), and net-section failure (NS), as illustrated in Figure 5 (a–d).

For single-screw connections, when the horizontal edge distance (e_3) was 15 mm, increasing the sheet thickness resulted in T-B becoming the dominant failure mode. However, for specimens with a 5.5 mm screw diameter, S was observed, while a 6.3 mm screw diameter maintained the T-B failure mode. In specimens with 1 mm sheet thickness and 7.5 mm horizontal edge distance, increasing the screw diameter shifted the failure mode from T-B to NS. Conversely, for a thicker sheet with a 5.5 mm screw, the observed mode was T-S, which transitioned to NS as the screw diameter increased.

In two-screw configurations, for specimens with screws in vertical alignment and $e_3 = 15$ mm, increasing sheet thickness changed the failure mode from T-B to S. When $e_3 = 7.5$ mm, NS occurred. For specimens with screws in horizontal alignment, increasing sheet thickness caused the failure mode to evolve from T-B to T-S.

The results indicate that the failure mode of self-drilling screw connections in cold-formed steel members is not governed by a single parameter, but rather by the complex interaction of edge distance, sheet thickness, screw diameter, and screw arrangement. Notably, a reduction in horizontal edge distance critically influences connection behavior, often triggering more brittle modes such as NS, where the sheet weakens. Additionally, increasing sheet thickness and screw diameter generally shifts the failure mode from screw/sheet interaction to modes governed by the ultimate strength of either the screw or the sheet. These findings highlight that, in the design of such connections, it is essential not only to consider load-carrying capacity but also to carefully control the failure mode to ensure the desired ductile behavior.

(a) T-B type failure

(b) S type failure

(c) NS type failure

Figure 5. Types of failure modes of the test specimens.

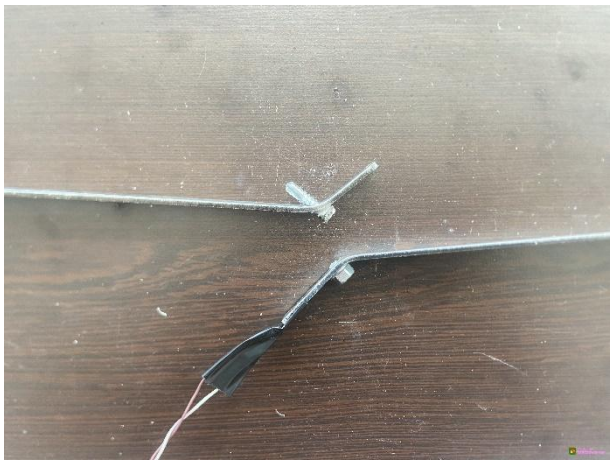

(d) T-S type failure

Figure 5 (continued). Types of failure modes of the test specimens.

Table 3. Test results.

Test Specimens	Screw Diameter, d (mm)	Thickness t_1-t_2 (mm)	Screw Number	Load Carrying Capacity P_{ns} (kN)	Failure Modes
1SC55EV30EH15T1-1	5.5	1-1	1	3.92	T-B
1SC63EV30EH15T1-1	6.3	1-1	1	4.16	T-B
1SC55EV30EH15T2-2	5.5	2-2	1	7.85	S
1SC63EV30EH15T2-2	6.3	2-2	1	8.39	T-B
1SC55EV30EH75T1-1	5.5	1-1	1	2.99	T-B
1SC63EV30EH75T1-1	6.3	1-1	1	3.08	NS
1SC55EV30EH75T2-2	5.5	2-2	1	5.56	T-S
1SC63EV30EH75T2-2	6.3	2-2	1	5.73	NS
2SCL55BW60EV30EH15T1-1	5.5	1-1	2	7.1	T-B
2SCL63BW60EV30EH15T1-1	6.3	1-1	2	7.43	T-B
2SCL55BW60EV30EH15T2-2	5.5	2-2	2	15.56	S
2SCL63BW60EV30EH15T2-2	6.3	2-2	2	15.11	S
2SCL55BW60EV30EH75T1-1	5.5	1-1	2	3.82	NS
2SCL63BW60EV30EH75T1-1	6.3	1-1	2	3.77	NS
2SCL55BW60EV30EH75T2-2	5.5	2-2	2	8.27	NS
2SCL63BW60EV30EH75T2-2	6.3	2-2	2	7.45	NS
2SCT55BW10EV30EH20T1-1	5.5	1-1	2	5.08	T-B
2SCT63BW10EV30EH20T1-1	6.3	1-1	2	5.02	T-B
2SCT55BW10EV30EH20T2-2	5.5	2-2	2	10.59	T-S
2SCT63BW10EV30EH20T2-2	6.3	2-2	2	11.15	T-S

4. NUMERICAL STUDIES

In this study, a numerical analysis was conducted using the finite element method (FEM) to investigate the structural behavior of self-drilling screw connections in cold-formed steel sheets and to validate the experimental findings. Finite element models were developed in ABAQUS [20] to simulate the load–displacement behavior and failure modes of the single-lap shear connections tested experimentally.

4.1. Geometry and Material Definition

The geometry of the finite element models was created based on the actual dimensions of the specimens used in the experimental study. To reduce modeling complexity and computational time, only the connection region and the critical stress zones of the steel sheets were considered, with a total modeled length of 150 mm. Screws were modeled to represent the head, shank, and diameter, but to optimize analysis time and avoid convergence issues associated with the highly complex mesh of screw threads, the screw surfaces were simplified as smooth (threadless). This approach provided an acceptable level of accuracy for global load–displacement behavior and connection capacity, while significantly improving computational efficiency.

Material models were defined using data obtained from tensile tests and the manufacturer's technical specifications. To accurately represent the material behavior during the localized necking phase, the true stress–strain curves used as input for the ABAQUS were defined to maintain an upward trend, ensuring that the increasing true stress reflects the actual reduction in the cross-sectional area until failure. The true stress–strain curves used to describe the nonlinear behavior of the steel sheets are presented in Figure 6. The material models for the finite element analysis were defined using the engineering stress-strain data obtained from the tensile tests summarized in Table 2. The engineering data were converted to true stress-strain curves for the plastic region by applying standard transformation equations (Eq. 1-2) prior to their use in ABAQUS [20].

$$\sigma_{\text{true}} = \sigma_{eng}\left(1 + \varepsilon_{eng}\right) \tag{1}$$

$$\varepsilon_{\text{true(pl)}} = \ln\left(1 + \varepsilon_{eng}\right) - \frac{\sigma_{\text{true}}}{\text{E}} \tag{2}$$

Here, σ_{true} represents true stress, $\varepsilon_{true(pl)}$ true strain, σ_{eng} engineering stress, ε_{eng} engineering strain and E Young's modulus.

The material properties of the screws were obtained from the manufacturer's technical datasheets. The screws were modeled with a Young's modulus of 210,000 MPa, Poisson's ratio of 0.3, yield strength of 833 MPa, and tensile strength of 1030 MPa. The mass density of the screws was taken as 7.98×10^{-5} N/mm³, consistent with that of the steel sheets.

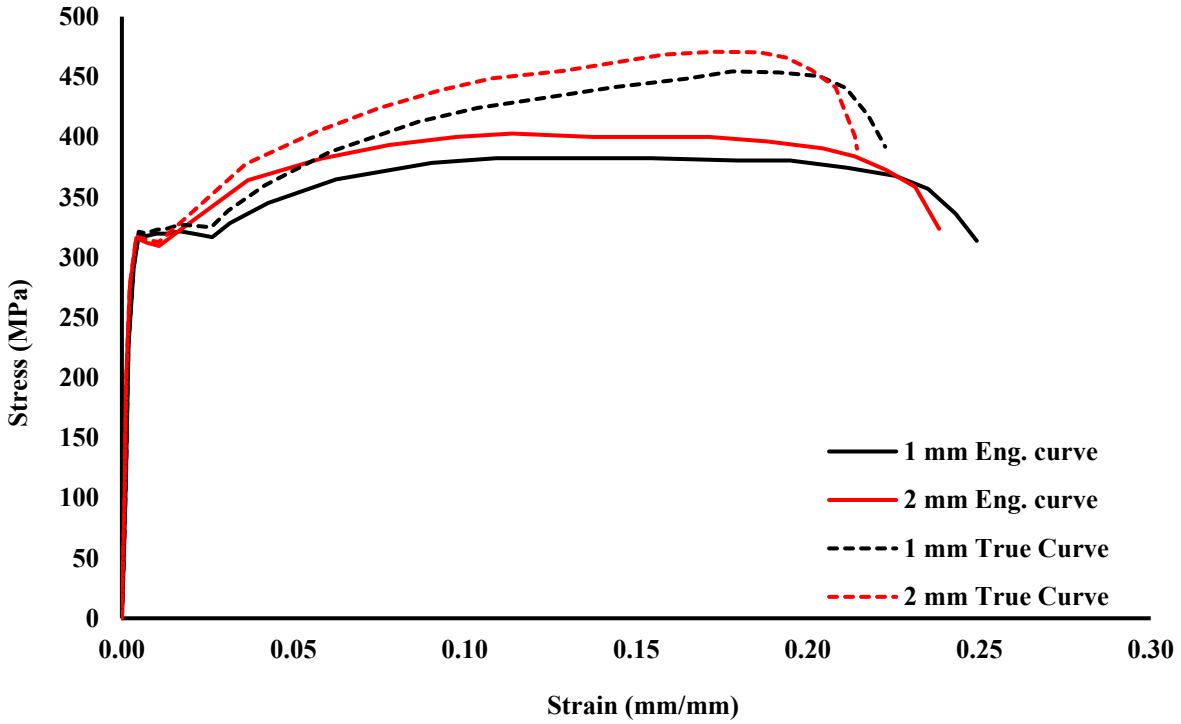

Figure 6. True stress-strain curves.

4.2. Mesh Type

In the finite element analysis of screw-connected steel sheets, three-dimensional eight-node reduced integration solid elements (C3D8R) were employed to model both the screws and the sheets. This element type was selected to ensure computational efficiency while maintaining adequate accuracy. Based on preliminary analyses and similar studies reported in the literature, the mesh size in the connection region was set to 0.5 mm × 0.5 mm.

To optimize computational time, only the screws and the critical zones directly in contact with the screws were modeled using this fine mesh. In contrast, regions with relatively lower stress concentrations were meshed at 3 mm × 3 mm. This approach effectively balanced model accuracy and analysis efficiency. The overall mesh configuration of the model is illustrated in Figure 7.

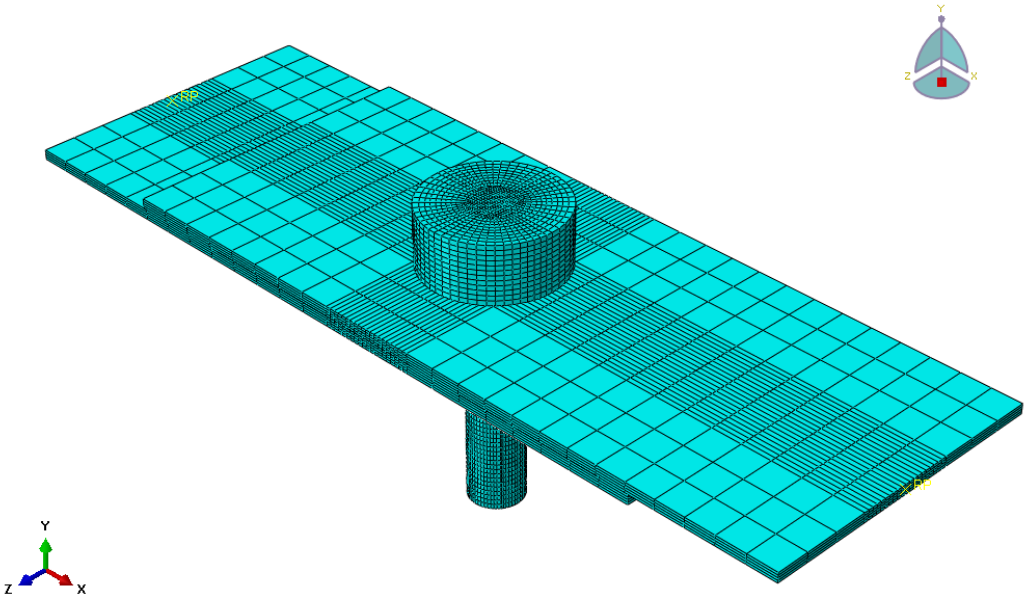

Figure 7. Mesh arrangements of steel plate and screw.

4.3. Boundary Conditions and Contact Modelling

In the finite element models, boundary conditions were defined to replicate the experimental setup. For the stationary plate representing the fixed support, all translational and rotational degrees of freedom (U_x=U_y=U_z=UR_x=UR_y=UR_z=0) were fully constrained. For the movable plate where the load was applied, only the U_y and U_z translations were constrained. These boundary conditions were implemented using a "Coupling Behavior (Structural Distributing)" constraint as illustrated in Figure 8.

The loading was applied by defining a reference point attached to the movable plate, simulating the experimental conditions. The load was then applied to this reference point using the same Coupling Behavior (Structural Distributing) constraint to ensure controlled application.

Contact interactions in the model were defined using the Surface-to-Surface Contact approach along with the Kinematic Contact Method. Separate contact properties were assigned for sheet-to-sheet, sheet-hole-to-screw shank, and screw head-to-sheet interactions. The tangential behavior of the contacts was modeled using the Penalty method, with a friction coefficient of 0.3 for sheet-to-sheet and sheet-hole-to-screw shank interactions, and 1.0 for screw head-to-sheet contact. The normal behavior was defined as Hard Contact, allowing separation after contact.

This detailed modeling approach enables a realistic simulation of contact-based behaviors in the assemblies (Figure 8).

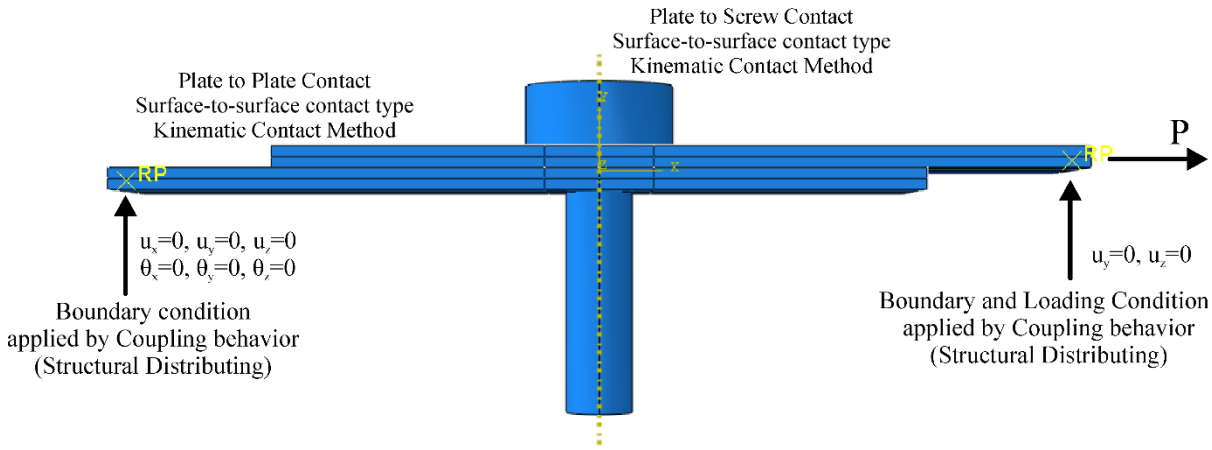

Figure 8. Boundary conditions and contact modelling.

4.4. Analysis Method

Numerical analyses of cold-formed steel specimens with screw connections were conducted using the ABAQUS/Explicit solver to simulate their nonlinear structural behavior under quasi-static loading conditions. The Explicit approach was chosen to overcome potential convergence issues arising from complex contact interactions effectively.

The load was applied incrementally and displacement-controlled to a reference point attached to the movable plate. This method enabled the precise tracing of the load-displacement response, including the post-peak behavior, and allowed for the accurate identification of failure modes. The analysis was continued until a significant drop in load, indicative of structural failure, was observed.

4.5. Validation of the Numerical Models

To evaluate the accuracy and reliability of the developed finite element models, the results from the numerical analyses were compared with the experimental findings. The comparison focused on both the load-carrying capacity (Pns) and the observed failure modes. The experimental and numerical load capacities and failure modes for all test specimens are detailed in Table 4.

As shown in Table 4, there is a high level of agreement between the numerical load capacities (Pns,FEM) and the experimental results (Pns,TEST). For the 20 specimens analyzed, the ratio Pns,FEM/Pns,TEST ranged from 0.89 to 1.10, with an average of 0.98 and a coefficient of variation (COV) of 0.06. The proximity of the average value to 1.00, combined with the low COV, indicates that the finite element models predict the load-carrying capacity with high accuracy and consistency. A comparison of the experimental and numerical load–displacement curves is presented in Figure 9.

Furthermore, the numerical models were generally successful in predicting the failure modes observed experimentally. Dominant failure modes such as T-B, S, and NS were accurately captured in the simulations. Minor discrepancies were observed in a few specimens, for instance, 1SC63EV30EH75T1-1 and 1SC63EV30EH75T2-2, where the experimentally observed NS mode was predicted as T-B in the numerical analysis. Such deviations may be attributed to the simplified modeling of screw threads or the effects of the material failure criteria. A comparison of the failure modes is shown in Figure 10.

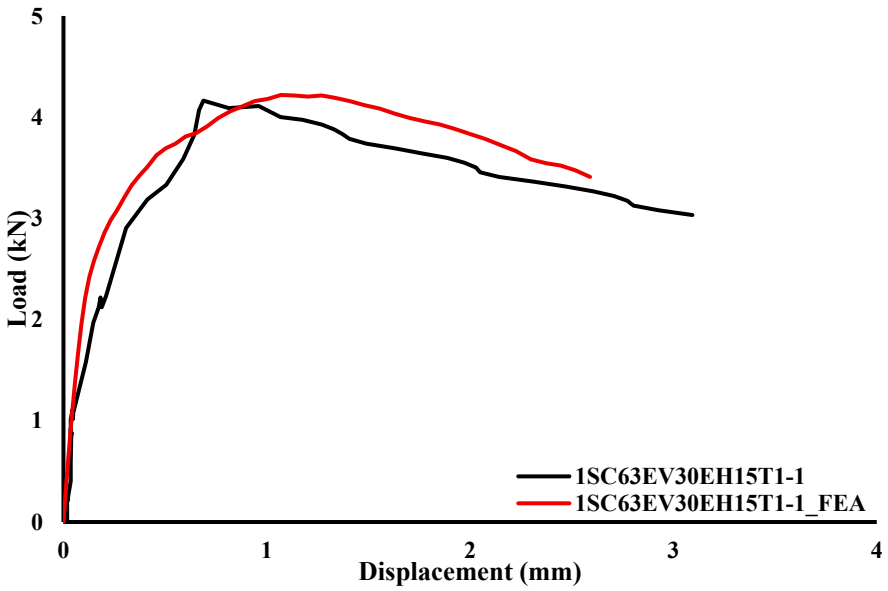

(a) *1SC63EV30EH15T1-1 test member*

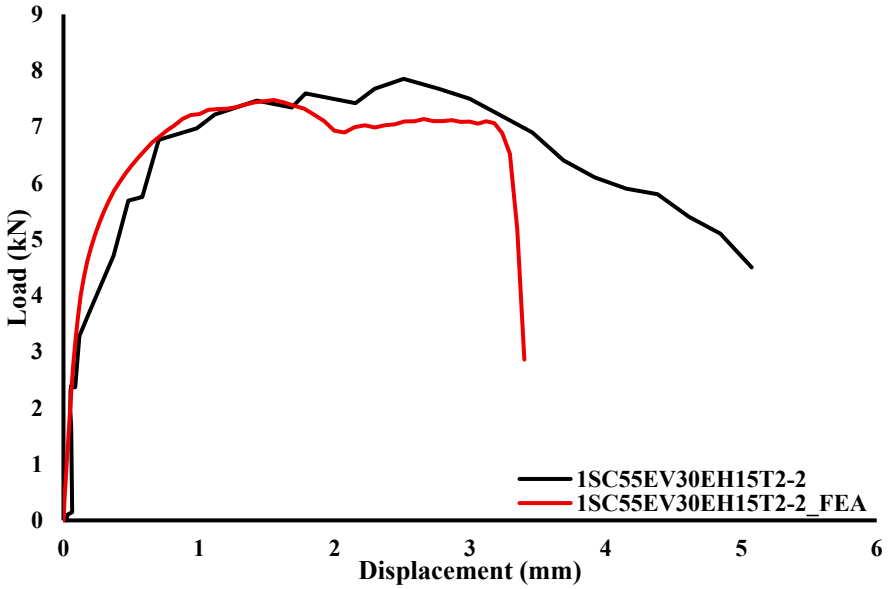

(b) 1SC55EV30EH15T2-2 test member

Figure 9. Load-displacement curves for test and FEA.

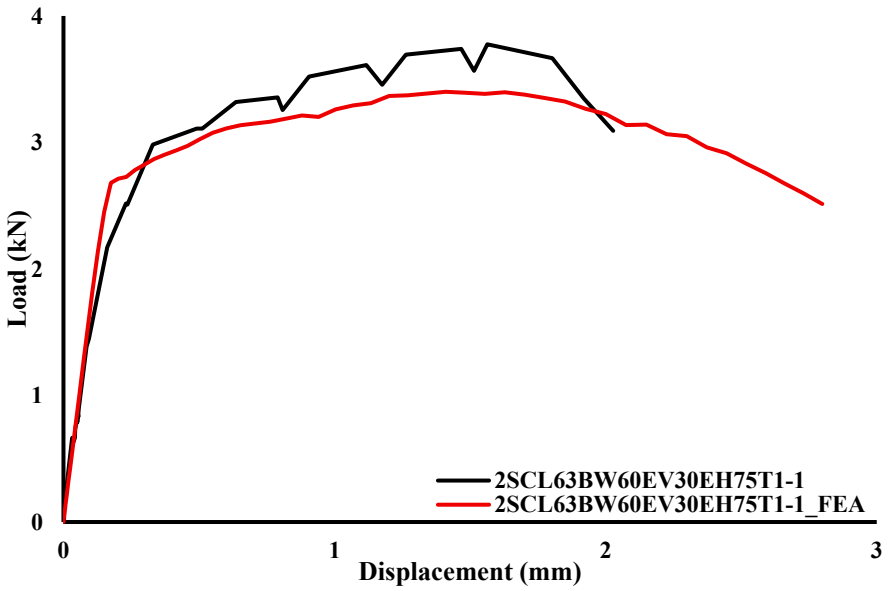

(c) 2SCL63BW60EV30EH75T1-1 test member

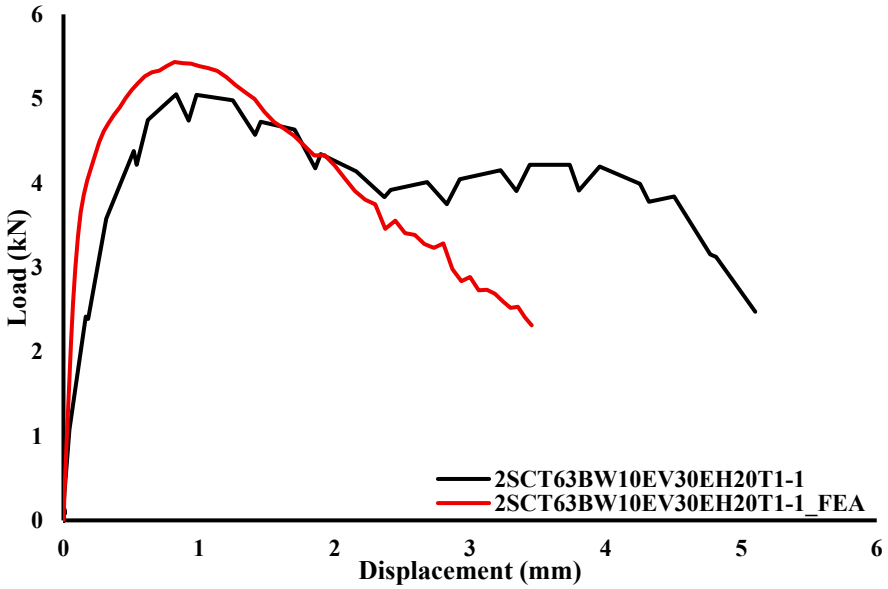

(d) 2SCT63BW10EV30EH20T1-1 test member

Figure 9 (continued). Load-displacement curves for test and FEA.

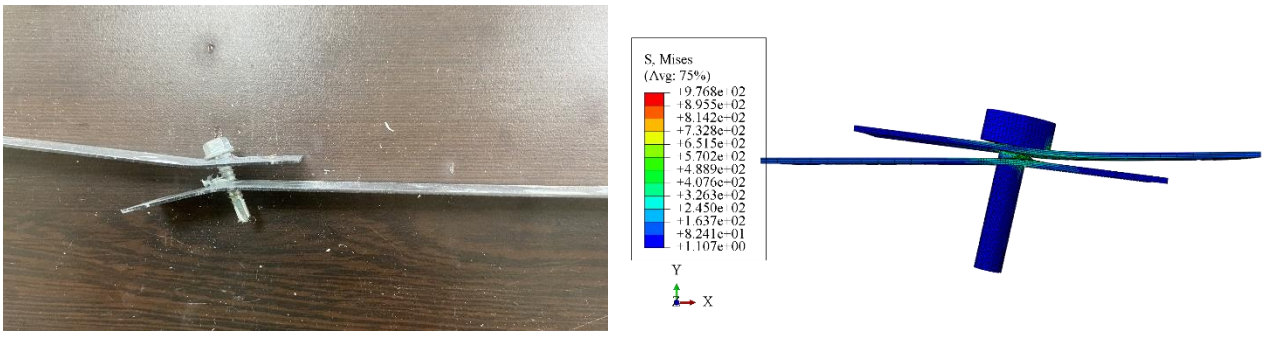

(a) T-B type failure

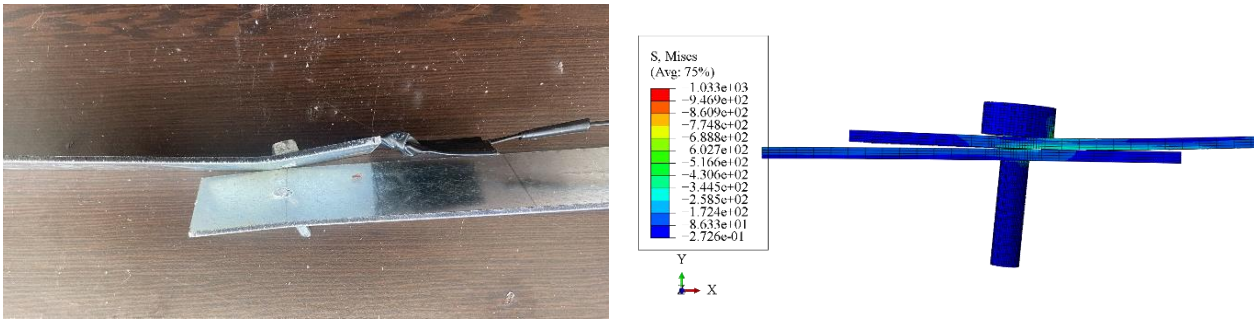

(b) S type failure

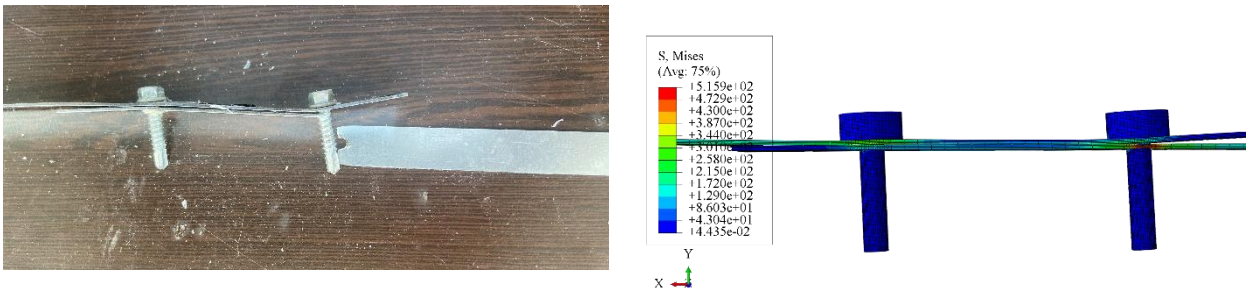

(c) NS type failure

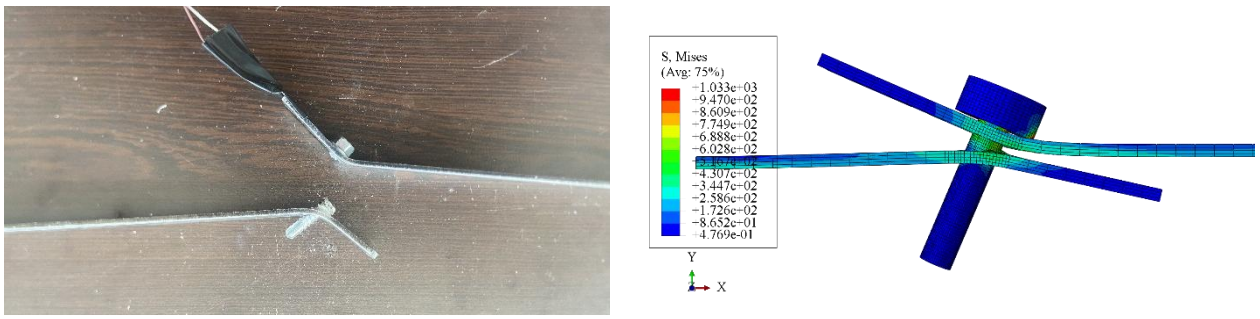

(d) T-S type failure

Figure 10. Comparison of failure modes for test vs numerical model.

Table 4. Comparison of test and numerical results.

Test Specimens	$P_{ns,TEST}$ (kN)	Failure Modes (TEST)	$P_{ns,FEM}$ (kN)	Failure Modes (FEM)	$P_{ns,FEM}/P_{ns,TEST}$
1SC55EV30EH15T1/1	3.92	T-B	3.87	T-B	0.99
1SC63EV30EH15T1/1	4.16	T-B	4.21	T-B	1.01
1SC55EV30EH15T2/2	7.85	S	7.47	S	0.95
1SC63EV30EH15T2/2	8.39	T-B	7.93	T-B	0.95
1SC55EV30EH75T1/1	2.99	T-B	2.92	T-B	0.98
1SC63EV30EH75T1/1	3.08	NS	2.87	T-B	0.93
1SC55EV30EH75T2/2	5.56	T-S	5.59	T-S	1.00
1SC63EV30EH75T2/2	5.73	NS	5.43	T-B	0.95
2SCL55BW60EV30EH15T1/1	7.1	T-B	7.46	T-B	1.05
2SCL63BW60EV30EH15T1/1	7.43	T-B	7.43	T-B	1.10
2SCL55BW60EV30EH15T2/2	15.56	S	14.52	S	0.93
2SCL63BW60EV30EH15T2/2	15.11	S	14.68	S	0.97
2SCL55BW60EV30EH75T1/1	3.82	NS	3.66	NS	0.96
2SCL63BW60EV30EH75T1/1	3.77	NS	3.4	NS	0.90
2SCL55BW60EV30EH75T2/2	8.27	NS	7.38	NS	0.89
2SCL63BW60EV30EH75T2/2	7.45	NS	6.8	NS	0.91
2SCT55BW10EV30EH20T1/1	5.08	T-B	5.33	T-B	1.05
2SCT63BW10EV30EH20T1/1	5.02	T-B	5.43	T-B	1.08
2SCT55BW10EV30EH20T2/2	10.59	T-S	10.81	T-S	1.02
2SCT63BW10EV30EH20T2/2	11.15	T-S	10.94	T-S	0.98
Mean					0.98
COV					0.06

5. CONCLUSIONS AND RECOMMENDATIONS

In this study, the shear behavior of cold-formed steel (CFS) plates connected with closely spaced self-drilling screws was investigated through both experimental testing and numerical analysis. Based on the experiments conducted on a total of 20 single-lap connection specimens and the developed finite element models, the following conclusions were drawn:

- Increasing the plate thickness was identified as the most effective parameter, nearly doubling the load-carrying capacity of the connections.
- An increase in screw diameter had a limited effect on the connection capacity.
- A reduction in horizontal edge distance had a critical impact on the connection performance. Furthermore, insufficient edge distance fundamentally alters the failure mechanism of the connections. While specimens with adequate edge distance typically exhibited tilting and bearing (T-B), reducing the edge distance triggered a transition toward net-section failure (NS).
- The developed finite element models accurately predicted the load–displacement curves, load-carrying capacities, and failure modes, confirming their reliability as a tool for future parametric studies.

Based on these findings, the following recommendations are suggested for the design of CFS screw connections:

- Future studies should consider the uneven distribution of load among screws (especially group effect), particularly when assessing the capacity of multi-screw connections.
- The validated finite element model from this study can be used to explore connection behavior under geometries, materials, and loading conditions not covered by current standards, thereby contributing to the improvement of existing design guidelines.

Acknowledgements

This study has been supported by the Scientific Research Projects Coordination of Aksaray University under project number BAP- 2025–030. The authors would also like to thank Prof. Dr. Babür DELİKTAŞ, Faculty of Engineering, Department of Civil Engineering, Bursa Uludag University, for his help in numerical analysis.

Conflict of Interest Statement

There is no conflict of interest between the authors.

Statement of Research and Publication Ethics

The study is complied with research and publication ethics.

Artificial Intelligence (AI) Contribution Statement

During the preparation of this work the authors used Grammarly in order to improve readability and language. After using this tool/service, the authors reviewed and edited the content as needed and take full responsibility for the content of the publication.

Contributions of the Authors

Oruç, Ramazan: Writing – review & editing, Writing – original draft, Visualization, Supervision, Software, Methodology, Investigation, Conceptualization.

Bölükbaş, Yakup: Writing – review & editing, Writing – original draft, Visualization, Supervision, Software, Methodology, Investigation, Conceptualization.

REFERENCES

[1] M. T. Huynh, C. H. Pham, and G. J. Hancock, "Experimental behaviour and modelling of screwed connections of high strength sheet steels in shear," *Thin-Walled Structures*, vol. 146, 2020. doi: 10.1016/j.tws.2019.106357.

[2] European Union, *EN 1993-1-3 (2006): Eurocode 3: Design of steel structures - Part 1-3: General rules - Supplementary rules for cold-formed members and sheeting*, Brussels: The European Union Per Regulation, 2006.

[3] American Iron and Steel Institute (AISI), *AISI S100-16: North American Specification for the Design of Cold-Formed Steel Structural Members*, Washington, DC: American Iron and Steel Institute, 2016.

[4] C. A. Rogers and G. J. Hancock, "Screwed connection tests of thin G550 and G300 sheet steels," *Journal of Structural Engineering*, vol. 125, no. 2, pp. 128-136, 1999. doi: 10.1061/(ASCE)0733-9445(1999)125:2(128).

[5] M. T. Huynh, C. H. Pham, and G. J. Hancock, "Design of screwed connections in cold-formed steels in shear," *Thin-Walled Structures*, vol. 154, 2020. doi: 10.1016/j.tws.2020.106817.

[6] K. Y. Cai and H. X. Yuan, "Testing, numerical and analytical modelling of self-drilling screw connections between thin steel sheets in shear," *Thin-Walled Structures*, vol. 182, 2023. doi: 10.1016/j.tws.2022.110292.

[7] S. S. Chao, L. F. Lu, and H. H. Wu, "Shearing Bearing Capacity of Screwed Connections of Thin Steel Sheets," *International Journal of Steel Structures*, vol. 19, no. 2, pp. 577-590, 2019. doi: 10.1007/s13296-018-0144-5.

[8] H. W. Zhang, F. L. Wang, J. Yang, and X. E. Wang, "Evaluation on the behaviour of screwed CFS joints subjected to combined loading," *Journal of Constructional Steel Research*, vol. 180, 2021. doi: 10.1016/j.jcsr.2021.106582.

[9] S. Liu, R. Q. Feng, and Y. T. Zhong, "Experimental and numerical studies of screwed connections with hot-rolled steel plate and cold-formed steel sheet," *Structures*, vol. 51, pp. 311-319, 2023. doi: 10.1016/j.istruc.2023.03.063.

[10] K. Roy, H. H. Lau, T. C. H. Ting, R. Masood, A. Kumar, and J. B. P. Lim, "Experiments and finite element modelling of screw pattern of self-drilling screw connections for high strength cold-formed steel," *Thin-Walled Structures*, vol. 145, 2019. doi: 10.1016/j.tws.2019.106393.

[11] L. F. Lu, D. Wang, W. Wang, H. H. Wu, K. Ding, K. K. Darkwah, and H. W. Yan, "Shear bearing capacity of Self-drilling screw group connections of CFS sheets," *Structures*, vol. 35, pp. 160-171, 2022. doi: 10.1016/j.istruc.2021.10.096.

[12] I. Rouaz, S. A. Rafa, H. Bouzid, M. Saidani, and A. Ahmed-Chaouch, "Investigation of screw assembly on cold-formed steel members: experimental and numerical studies," *Asian Journal of Civil Engineering*, vol. 25, no. 4, pp. 3349-3362, 2024. doi: 10.1007/s42107-023-00983-w.

[13] W. Lu, P. Mäkeläinen, J. Outinen, and Z. C. Ma, "Design of screwed steel sheeting connection at ambient and elevated temperatures," *Thin-Walled Structures*, vol. 49, no. 12, pp. 1526-1533, 2011. doi: 10.1016/j.tws.2011.07.014.

[14] S. Yan and B. Young, "Screwed connections of thin sheet steels at elevated temperatures - Part I: Steady state tests," *Engineering Structures*, vol. 35, pp. 234-243, 2012. doi: 10.1016/j.engstruct.2011.10.030.

[15] S. Yan and B. Young, "Screwed connections of thin sheet steels at elevated temperatures - Part II: Transient state tests," *Engineering Structures*, vol. 35, pp. 228-233, 2012. doi: 10.1016/j.engstruct.2011.10.027.

[16] S. T. Vy and M. Mahendran, "Screwed connections in built-up cold-formed steel members at ambient and elevated temperatures," *Journal of Constructional Steel Research*, vol. 192, 2022. doi: 10.1016/j.jcsr.2022.107218.

[17] L. Yin, K. Liu, W. Chen, J. H. Ye, M. Zhang, Z. Y. Fang, and J. B. P. Lim, "Behaviour of screwed connections in cold-formed steel sheets at elevated temperatures," *Thin-Walled Structures*, vol. 213, 2025. doi: 10.1016/j.tws.2025.113317.

[18] American Iron and Steel Institute (AISI), *AISI S905-13: Test Standard for Cold-formed Steel Connections*, Washington, DC: American Iron and Steel Institute, 2013.

[19] Turkish Standards Institution, *TS EN ISO 6892-1, Metallic materials - Tensile testing - Part 1: Method of test at room temperature (ISO 6892-1:2019)*, Ankara: Turkish Standards Institution, 2020.

[20] ABAQUS Inc., *ABAQUS Analysis User's Manual-Version 6.14-2*, USA: ABAQUS Inc., 2018.